Chapter 14

Rice Plant Height Monitoring from Space with Bistatic Interferometry

Cristian Rossi

Additional information is available at the end of the chapter

http://dx.doi.org/10.5772/65868

Abstract

This chapter provides an overview of the possibility to derive paddy rice plant heights with spaceborne bistatic SAR interferometry (InSAR). By using the only available interferometer in space, TanDEM-X, an investigation of rice crops located in Turkey is performed. Before analyzing the main outcomes, an introduction to the generation of elevation models with InSAR is provided, with a special focus on the agricultural land cover. The processing chain and the modifications foreseen to properly produce plant elevations and a roadmap for the quality assessment are described. The results obtained, with a very high interferometric coherence supporting an accurate estimation due to a limited electromagnetic wave penetration into the canopy, support a temporal change analysis on a field-by-field basis. For the purpose, an automatic approach to segment the fields without external auxiliary data is also provided. The study is concluded with an analysis of the impact of the wave polarization in the results.

Keywords: SAR, InSAR, DEM, TanDEM-X, agricultural remote sensing

1. Introduction

Remote sensing is a mature technology for the observation of natural environmental changes. In terms of agricultural monitoring applications, radar sensors differ from optical, multispectral, and thermal sensors for two main reasons: (1) radar systems can collect imagery independent of solar illumination and cloud cover. This is particularly relevant for countries affected by heavy precipitations during the plant growing stages. (2) The system measures amplitudes and phases of the backscattered signal, yielding the joint derivation of absolute ranging and backscattering coefficients. Both of them can be exploited to derive the plant height, as explained in the following.

The investigation presented in this chapter is performed for paddy-rice fields, even though in principle it can be generalized for other vertical-oriented vegetation crops. The relevance of the

study comes from economical and geo-political aspects. According to the Food and Agricultural Organization (FAO), rice is one of the most valuable livestock products in the world, with a production of more than 700 million tons per year [1]. As a consequence, a big interest of international agencies, insurance companies, and governments are posed on this staple food. For instance, politicians and governments are particularly interested in the monitoring of farming practices and land control, e.g., to check for hidden and/or spoofed markets. Insurance companies are interested in forecasting coverage costs by knowing the status of crops at the moment of possible flooding. Agencies would like to regulate the product import/export based on the yield estimation and the current demand. The possibility to globally monitor paddies, by providing the growth status and field borders, is then very relevant.

This global monitoring can be ensured with the utilization of synthetic aperture radar (SAR) systems. SAR images have been already used for several campaigns for crop inspections (e.g., [2–6]). Many possible measures of rice growth such as canopy height, LAI, biomass, etc. are considered in the works cited above. Among them, canopy height is the most direct measurement and has direct relationship with growth rate, especially in the early growing stage. There are three techniques that can be employed to derive the rice plant height with SAR data: single-image backscatter analysis, SAR interferometry (InSAR), and Polarimetric SAR Interferometry (PolInSAR).

1.1. Single-image backscatter analysis

A practiced strategy relies in finding the correlation between canopy height and backscattering coefficients, although the scattering process is not a function depending only on crop height. In fact, an indirect relationship can be assessed. The electromagnetic scattering of the plant is a function of intricate interrelations among physical parameters of rice [7]. By taking into account the different scattering mechanisms involved in the acquisition process, the system parameters, and the physical properties of the plant, it is in principle possible to invert a complex model and derive, among other parameters, also the plant height. Nevertheless, only a few studies are reported in the literature for this purpose and they are based on experimental data sets and locally selected thresholds, thus limiting their accuracy and not being suitable for operational processors commanded to process various data sets [8].

1.2. SAR interferometry (InSAR)

Direct height information can be instead derived with the cost of two SAR images, by employing the interferometric technique [9]. In contrast to the single-image backscattering information, InSAR exploits the phase information embedded in the received signal. From an agricultural application point of view, in the literature, interferometric phase information has been employed by making use of the coherence as in Refs. [10, 11]. In these works, most of the attention has been given on the accuracy of the interferometric phase for the C-band European remote sensing (ERS) tandem data set. However, ERS data spatial resolution is very low, about 30 m, not being able to tackle the physical-based spatial heterogeneity problem in paddy-rice fields. Two other limiting factors are the wave penetration at C-band, causing an underestimation in volume deviations, and the nonzero temporal baseline, causing unreliable interferometric

http://dx.doi.org/10.5772/65868

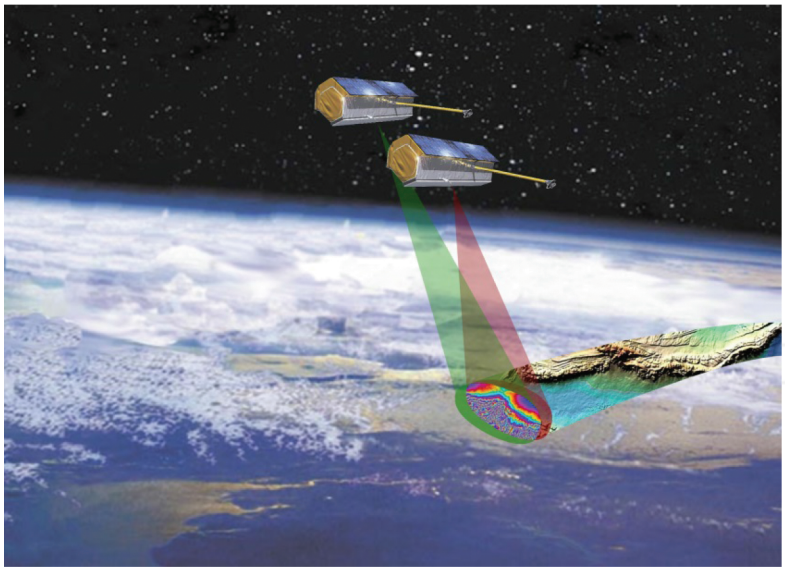

Figure 1. Artist's view of the TanDEM-X mission (©DLR).

phase information. A promising SAR concept to attenuate these limitations is TanDEM-X. An artist's view of the mission is sketched in **Figure 1**. TanDEM-X is an innovative mission, started in 2010 with the launch of a twin satellite (TDX-1) placed in close formation with the TerraSAR-X satellite (TSX-1). The main mission objective is the generation of a global digital elevation model (DEM) with HRTI-3 accuracy standards [12]. The mission acronym says just that: *TerraSAR-X add-on for Digital Elevation Measurement*. By definition, the DEM renders the height of what lays on the Earth at a given position, thus, also paddy-rice plants. A study about the accuracy of the DEM for crops is the main objective of this chapter.

The standard TanDEM-X mode of operation is bistatic, i.e., established on a single signal transmission and a dual reception. The chapter title term *bistatic interferometry* refers to this technique. The satellite transmitting and receiving the signal is also named *active* satellite, while the one only receiving the signal is named *passive* satellite. By doing so, strong DEM error sources for agricultural mapping such as atmospheric artifacts or temporal changes are avoided. Moreover, the wave penetration into the canopy is strongly limited with the employed wavelength of about 3.1 cm (X-band). Among other possible operation modes, it is worth mentioning the *monostatic* one, where the two satellites are run independently. This is the case of repeat-pass acquisitions, i.e., acquisitions taking place at different times. The potentials of TanDEM-X to render paddy-rice heights have been reported in [13, 14]. The flexible commanding yields the acquisition of several DEMs over the same area in a short revisit time, thus allowing a temporal study about the plant growth. This chapter takes inspiration from these works and revisits the results with an extended introduction about the uncertainty assessment of agricultural DEMs generated with bistatic interferometry.

1.3. Polarimetric SAR interferometry (PolInSAR)

The last technique taken into consideration for plant height derivation is Polarimetric InSAR (PolInSAR) [15]. PolInSAR requires multiple-polarized SAR images. Like the single-image backscatter image analysis, the PolInSAR height estimation is also based on scattering models. In particular, these models relate the crop height to the interferometric coherence, and they vary depending on the physical structure of the plant [16]. A limitation of this technique is the required geometrical configuration of the satellites. Indeed, to obtain the required sensitivity of a few centimeters for plants growing to about 1 m, a spatial separation between satellites (also called *baseline*) of some kilometers is required [16]. This limitation strongly impact on the applicability to spaceborne systems. The first demonstration of usage has been reported with an airborne system [17].

This chapter is organized in the following way: Section 2 presents the system employed for the height derivation and provides an overview of bistatic interferometry. Section 3 applies the technique to the mapping of paddy-rice and presents and discusses the results. Section 4 deals with the impact of the wave polarization in the results and Section 5 traces the conclusions.

2. DEM generation with bistatic interferometry

A digital elevation model is a model describing the topographical variations of the Earth. Terrain height is the main information. The elevation is generally given above a certain level, e.g., a geodetic datum. For instance, TanDEM-X elevations are over the WGS84 ellipsoid. DEMs can be generated with various sensors, such as optical, LiDAR (Light Detection and Ranging), and SAR.

Stereo photogrammetry is the standard technique to generate DEMs with optical data. It refers to the technique of measuring the position of Earth points from a set of photographs—minimum two [18]. LiDAR (Light Detection and Ranging) is another popular system to produce DEMs [19]. It is an active system based on a pulse/CW laser employed to determine the distance between sensor and target. This technology reached its maturity in the 1990s and nowadays several companies offer laser surveys with an airborne system. As for LiDAR, SAR is an active system, i.e., based on the transmission and reception of signals. The whole process is coherent, i.e., established on the use of both amplitude and phase information. Several studies have been reported in the literature. For instance, successful usage of photogrammetry and laser scanning for crop height monitoring can be found in Refs. [20, 21], respectively.

In contrast with LiDAR, which determines a 3D location from one range measurement and 2D pointing angles, the InSAR 3D positioning relies on two antenna locations and on the measure of the interferometric unwrapped phase. The processing from SAR raw data to DEM is shown in **Figure 2**.

A complete description of the processing steps is out of the scope of this chapter and can be found in several articles and books, e.g., [9, 22]. Instead, their main characteristics and modification adapted to the mapping of agricultural crops are outlined in Section 2.1.

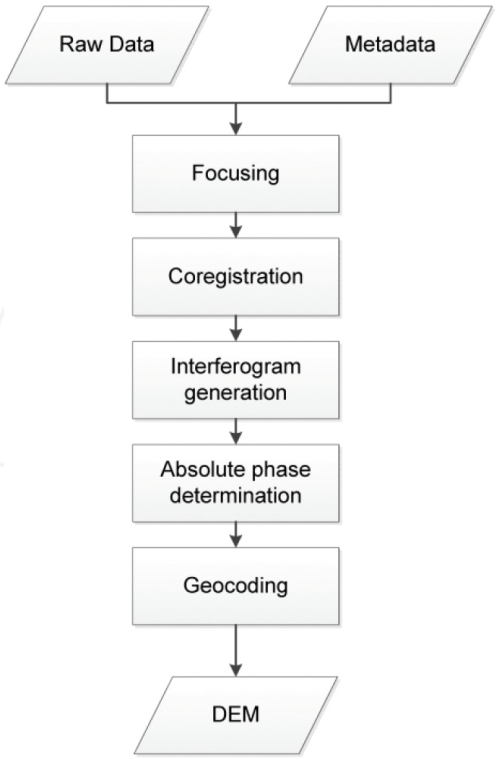

Figure 2. Flowchart of a typical InSAR processing chain finalized to DEM generation from SAR raw data.

2.1. InSAR processing steps

Agricultural crops are not a particularly difficult terrain to map and generally do not require dedicated processing solutions (see also Section 2.2) or modification to nominal InSAR processors. The processor used for the generation of the results presented in this chapter is the integrated TanDEM-X processor (ITP) [23, 24]. ITP is the operational processor employed in the German Aerospace Center (DLR) for the generation of TanDEM-X products. In the following, a brief description of the processing stages shown in **Figure 2** is provided with a special focus on the crop elevation modeling.

Focusing. Focusing is the process to form a SAR image from raw data [25]. The SAR image is a bidimensional complex array. The along-track dimension is named *azimuth*, while the across-track is named *range*. The conversion from pixel value to physical backscatter is also called radiometric calibration and is performed as:

$$\sigma^0 = (k|x|^2 - \beta_N)\sin\theta_i \tag{1}$$

where σ^0, or *Sigma Nought*, is the measure of the radar return, k is a sensor-dependent calibration factor, x is the pixel value after SAR focusing, β_N, or *Noise Equivalent Beta Naught*,

equivalent beta naught, represents the noise contribution into the signal and it is usually annotated in the SAR product, and θ_i is the local incidence angle. Since rice paddies develop in locally flat terrain, θ_i is equal to θ_l, the radar looking angle.

In the bistatic interferometric scenario, the focusing operation is performed for the active channel, generating the *master* image, and for the passive channel, generating the *slave* image.

Coregistration. Coregistration has the objective to obtain a precise sample-overlap between two SAR images. A typical algorithm employed for coregistering SAR data is the crosscorrelation [23]. No peculiar algorithmic issues are expected for paddies.

Interferogram generation. The interferogram, generated by complex conjugate multiplication of the two coregistered images, is the main product for the DEM generation, since its phase is directly related to the terrain height. Typically, to reduce speckle noise, a multilooking process is implemented. For the considered agricultural scenario, an efficient moving-average 2D window is sufficient. The number of looks used in the processing defines an important DEM parameter, the horizontal resolution.

Horizontal resolution (Ω_r). Ω_r represents the minimum resolvable distance between two objects at different height. It is determined as:

$$\Omega_r = \frac{n_{az}\delta_{az}^{gr} + n_{rg}\delta_{rg}^{gr}}{2} \tag{2}$$

where n_{az} and n_{rg} are the azimuth and range independent number of looks and δ_{az}^{gr} and δ_{rg}^{gr} represent the single SAR pixel azimuth and range ground resolution. The independent number of range and azimuth looks is a function of the looks used in the multilooking process [12]. Ω_r represents the average of the range and azimuth interferogram resolutions.

Absolute phase determination. The SAR interferometric technique is based on the exploitation of the complex interferogram. The interferogram is defined through phase principal values, with values ranging into the interval (-π,+π]. A critical stage of the interferometric chain is the absolute phase retrieval given the wrapped interferogram phase. This process, named *phase unwrapping*, is one of the most delicate of the whole processing chains. It consists, for every interferogram pixel, in the estimation of the number of phase cycles to be added to the wrapped value. The topographic phase ϕ_{top}, also called absolute unwrapped phase, is sensitive to the terrain height h through the relation

$$\frac{\partial\phi_{\text{top}}}{\partial h} = \frac{2\pi B_{\perp}}{\lambda r \sin\theta_l} = \frac{2\pi}{h_a} \tag{3}$$

where $B_{\perp}$ is the perpendicular baseline between satellites, λ is the wavelength, r is the slant range, and h_a is a useful derived parameter called height of ambiguity. The phase unwrapping step defines the unwrapped phase from the (wrapped) interferometric phase by adding an estimated integer number of cycles. The accuracy of this operation depends on h_a. Indeed, large heights of ambiguity data-takes are less prone to phase unwrapping errors that manifest

in the DEM as height discontinuities of multiples of h_a. In contrast, according to Eq. (3), small heights of ambiguity yield better results in terms of height sensitivity. For rice paddies, considering that the plant height is very small, growing up to 1–1.5 m, a small height of ambiguity would be preferred to obtain precise results. It has to be noticed that the unwrapping operation may even be not necessary for terrain height variation smaller than h_a, thus dramatically simplifying the overall InSAR processing. The nominal TanDEM-X ambiguity heights are around 40–60 m.

Finally, the unwrapped phase must be properly calibrated before the final geocoding step. The calibration involves the estimation of the *absolute phase offset*, which can be derived with external ground control points, with an external DEM, or with the DEM derived with the internal coregistration shifts, as in [24]. This DEM calibration is an important processing step for a multi-temporal elevation study like the one proposed in this chapter, since uncalibrated data provide misinterpretations of the geophysical outcomes. The method in [24], operationally employed for TanDEM-X production, should be actually discarded for multitemporal studies since every single absolute phase offset estimation is computed independently and is based on the local InSAR geometry. Error sources, such as baseline inaccuracies, may vary between geometries, thus producing absolute height differences between DEMs. For this reason, the calibration with a common reference is a more favorable solution. Obviously, the calibration points or region must be located outside the paddies and must consist of temporally stable elevations.

Geocoding. This processing step implies an absolute phase offset conversion in surface elevation and a georeference in a specific datum. It is a standard operation and no modifications are foreseen for agricultural mapping.

Figure 3 shows exemplary outputs from these processing stages for the test site considered in this chapter. Here, the master and slave amplitude channels in the top box reveal the changes in backscatter for the different land cover in the scene. The flattened interferogram in the second box, i.e., the interferometric phase compensated for the ellipsoidal height, shows the topographical variations.

One fringe represents a height variation equal to h_a, about 26 m in this case. The coherence gives a picture of the output quality, with very low values for low-backscatter areas (e.g., water) and high values in the central portion of the scene, covered by crops (see Section 2.2). The phase unwrapping, mandatory in this case due to the will to represent also the hilly portions of the scene at the upper and lower portions of the scene, is not creating artifacts, as can also be seen in the third box by the differential phase between the unwrapped phase and the equivalent phase generated with a reference elevation model, in this case represented by the Shuttle Radar Topography Mission (SRTM) [26] one. Finally, the generated DEM is displayed in a 3D view at the bottom of **Figure 3**.

2.2. DEM error sources and investigation

Although in principle every terrain can be mapped in elevation with InSAR, the obtained accuracy is strongly land cover dependent.

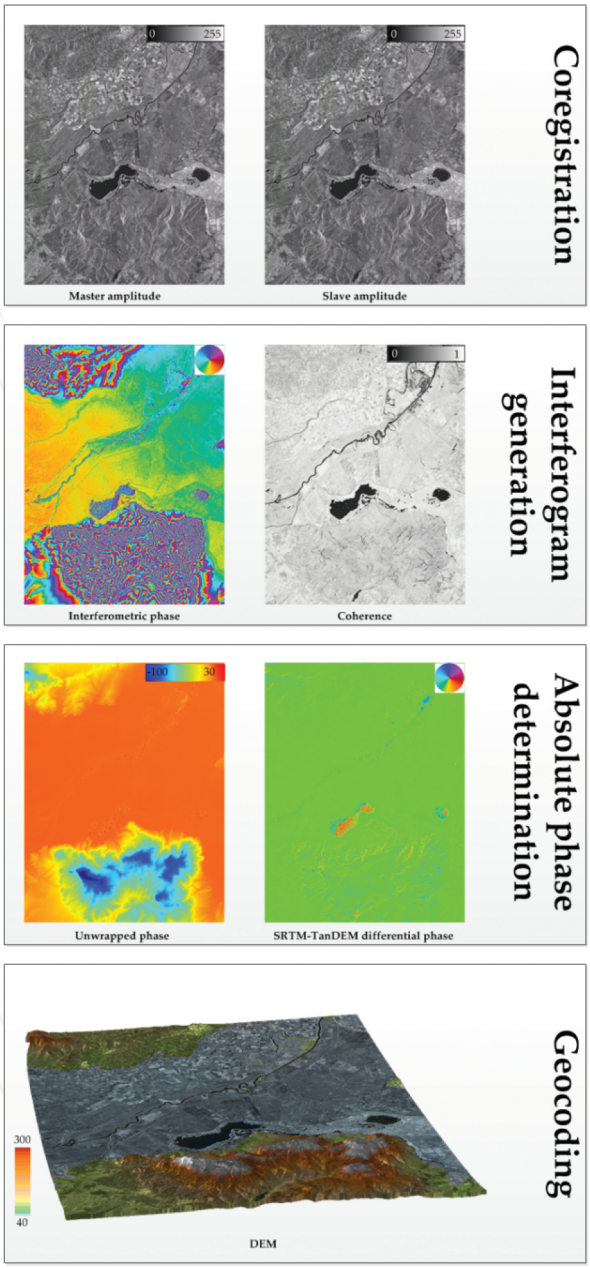

Figure 3. Interferometric processing example for the test site considered in the chapter. From the top, *coregistration stage*, with the master and slave amplitudes, *interferogram generation*, with the flattened interferometric phase, and the coherence, *absolute phase determination*, with the unwrapped phase and the differential phase between SRTM and TanDEM-X, and *geocoding*, with the final DEM.

2.2.1. Local geomorphology impact

Since SAR is a side-looking sensor, terrain slope impacts in the elevation model, with slopes that are even not representable due to the shadowing effect or to the multiple mapping in a single resolution cell (*layover*) [27]. Since agricultural crops are usually settled over flat or smooth terrains, the local geomorphology is not a source of error to take into account.

2.2.2. Plant structure impact

A relevant source of error for agricultural crops is instead the terrain itself. Being SAR an active system, i.e., transmitting and receiving energy, it is affected by wave propagation phenomena. Indeed, the wave propagates into the terrain depending on the material property [7, 31]. The measured height, i.e., the measured scattering phase center, depends on this property and in particular on the complex dielectric constant $\varepsilon_r = \varepsilon_r^{'} - j\varepsilon_r^{''}$. ε_r describes the medium characteristics in relationship to the electric field, i.e., how its power decreases in the medium where it travels. The loss of power density is described by the *penetration depth*

$$\delta_p = \frac{\lambda}{2\pi} \frac{\sqrt{\varepsilon_r^{'}}}{\varepsilon_r^{''}} \tag{4}$$

that is, the value for which the power density is reduced to 1/e. Deeper penetration is measured for low bandwidths and low moisture contents ($\varepsilon_r^{''}$ is proportional to moisture). The radar signal travels two times into the canopy, so that the equivalent penetration depth, or the scattering phase center location, is actually at $\delta_p/2\cos\theta_i$ below the top of the surface. In reality, the physical description of the electromagnetic interaction between the transmitted wave and the paddy-rice field is much more complex than that. For instance, also inhomogeneities of the inner portion of the plant and their integration into the SAR resolution cell contribute to the total signal extinction. This yields an overall loss of the interferometric coherence, which is also named *volume decorrelation* (see Section 2.2.3). Rather than inverting electromagnetic models and estimate the physical characteristics of the plants, this study aims to experimentally demonstrate the capabilities of the bistatic system in tracking the rice plant heights, thus indirectly deriving the impact of the signal extinction into the estimate.

2.2.3. Interferometric coherence

As aforementioned, in InSAR processors, the random error is measured by the coherence parameter. Coherence assesses the quantity of decorrelation that occurs between two SAR signals. It is defined as the crosscorrelation between two complex SAR images x_1 and x_2 and can be estimated as

$$\gamma = \left| \frac{\sum x_1 x_2 \exp\{-j\phi_{\text{known}}\}}{\sqrt{\sum |x_1|^2 \sum |x_2|^2}} \right|. \tag{5}$$

In Eq. (5), ϕ_{known} is a deterministic phase value, representing the topography and other known phase trends in the estimation window. This factor must be compensated to accomplish

stationarity [28]. Given the coherence, the marginal probability density function for the interferometric phase ϕ can be first estimated and the standard deviation of the interferometric phase $\sigma_\phi(r,a)$ can be then derived by integrating it [9]. The DEM standard error for every range and azimuth samples (r,a) is then calculated, according to Eq. (3), as

$$h_{\text{err}}(r,a) = \sigma_\phi(r,a)\frac{h_a}{2\pi}. \tag{6}$$

The error is proportional with the height of ambiguity: higher heights of ambiguity yield higher errors. To have an impression, for $h_a = 50$ m, a coherence value of 0.8 and 30 looks, the standard relative error is about 0.8 m. This error is only 0.3 m for $h_a = 20$ m.

Coherence can be decomposed in several factors [12], among which the volume decorrelation term, anticipated in Section 2.2.2, is the most relevant for rice paddies. To be noticed, coherence provides an estimate of the *relative* height error, as in Eq. (6). Relative height error refers to the error between two defined points in the elevation model, and sometimes it is specified as *point-to-point* error. It must not be confused with the *absolute* height error, i.e., how close the elevation cell is to the real height. A measure of the absolute error is described in the next section.

2.2.4. Difference with reference

The most straightforward way to evaluate the DEM quality is a direct comparison with references, in form of another DEM or in form of ground control points. It is clear that the reference must be originated from a different acquisition than the one under test. A typical solution for agricultural monitoring, as performed for the inspection presented in this chapter, is the setup of ground control points (GCPs) distributed in the field. More in detail, considering the current study, reference data has been collected in cooperation with the Istanbul Technical University (ITU). In particular, the state organization Trakya Agricultural Research Institute collected detailed ground truth in 8 fields with 4 independent samples per field during the growth cycle (May–October) of paddy-rice in 2013. Among the various gathered physical parameters, *height above ground* and *water* are the one of interest for the demonstration. The fieldwork dates are presented in **Figure 4** with the pictures taken during the campaign. To highlight the spatial variation in response to changes in agricultural practice, the first line in **Figure 4** shows the pictures taken from different fields on the same day. In this region, crops

Figure 4. Pictures taken for eight reference field during the ground truth data collection campaign [13]. The first line shows portion of the fields acquired on May 30, 2013, also illustrating the differences in agricultural practice. The second line shows the temporal evolution of field 8.

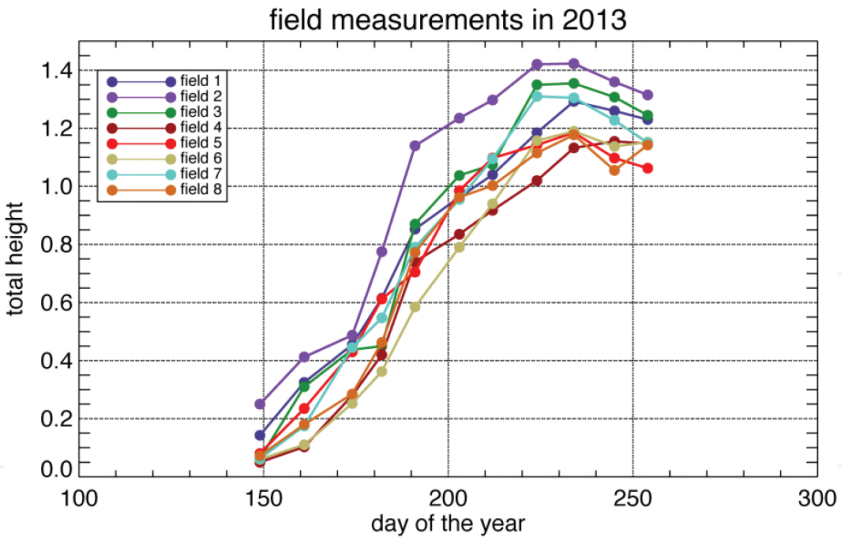

Figure 5. Relationship between the day of the year and the canopy height for the eight monitored fields [13].

are cultivated independently depending on the field owner's decision. Here, the sowing method is direct seeding by broadcasting, implying a random seeding instead of a regular straight-row one. This is a rather important point, since it highlights the expected randomness of the scattering. **Figure 5** shows the plots of the relationship between canopy height and day of the year obtained during the field works. Most fields were homogeneous and crops reached maximum height after flowering. Plant height ranges in between 0 and 140 cm.

The reference discrepancy needs quantification. In the mapping field, the standardized value for the vertical and horizontal positional accuracy is the root mean square error (RMSE). It is defined as

$$\mathrm{RMSE} = \sqrt{\frac{\sum_i^n (x_i - x_i^{\mathrm{REF}})^2}{n}} \tag{7}$$

where x_i and x_i^{REF} are the ith sample of the DEM and the reference, respectively. RMSE is of particular interest since it fully characterizes the error distribution, but just in case of normally distributed errors with zero-mean. Another used statistical descriptor of the DEM error is the standard deviation, which describes about the 68% of the normal population:

$$\hat{\sigma}_{\mathrm{err}} = \sqrt{\frac{\sum_i^n (x_i - x_i^{\mathrm{REF}} - \acute{e})^2}{n-1}} \tag{8}$$

where $\acute{e}$ is the mean error.

In this chapter, the validation is performed taking as reference the aforementioned ground campaign. The measures in Eqs. (5) and (6) present statistics of the absolute elevation error.

2.2.5. TanDEM-X specifications

DEM standards usually define a confidence interval, e.g., 90%, in order to discard outlier values. The positional accuracy is defined in the horizontal and vertical dimensions. The horizontal dimension determines the *absolute circular error*, i.e., the radius of a circle in which a specific feature must lie. The vertical dimension determines instead the *absolute linear error*, i. e., the elevation discrepancy between measure and ground truth. The TanDEM-X specification states a 90% absolute circular error of 10 m and a 90% absolute linear error of 10 m [12]. As for the absolute specification, the *relative circular error* describes how well the distance between two points in the model is represented. This horizontal error component has a 3 m specification for TanDEM-X at a 90% confidence. Similarly, the *relative linear error* describes the elevation error in between two points. For TanDEM-X, always at 90%, it shall be smaller than 2 m for slopes smaller than 20°, and smaller than 4 m for larger slopes.

3. Plant height derivation strategy and results

The test site chosen for the demonstration is the Lake Gala National Park, at the border between Greece and Turkey. The park is a particular wetland environment that consists of rivers, lakes, and agricultural fields (see **Figure 6**). In the last 50 years, topographical changes caused by heavy rain and debris flow were measured. More recently, the region is controlled by the Turkish government and made available for agricultural practice, in particular for paddy-rice. Considering the regional risk of debris flow, agricultural fields have to be monitored, controlling by this way the effect of flow. For instance, if the seeding has been affected from flow and irrigation, farmers can do transplanting again before it is too late for seeding. TanDEM-X monitoring is then particularly appealing for this test site.

3.1. Rice growth cycle

Before proceeding with technical details, the rice plant growth cycle shall be introduced. This cycle, from panicle initiation to maturing, lasts 110 to 250 days and can be divided in three stages: *vegetative, reproductive*, and *maturation*. Every stage is composed by different structural differences for the rice plant, described by a special scale called Biologische Bundesanstalt, bundessortenamt und CHemische industrie (BBCH) [29]. All the growing stages can be associated with the BBCH-scale, as shown in **Table 1**.

3.2. TanDEM-X dataset

Nine dual-pol TanDEM-X acquisitions have been acquired over the Lake Gala region in 2012 at an incidence angle of 36.8°. The data stack is processed with the integrated TanDEM-X processor [24]. The processor is commanded to generate HH (horizontal polarization in transmission and reception) and VV (vertical polarization in transmission and reception)

http://dx.doi.org/10.5772/65868

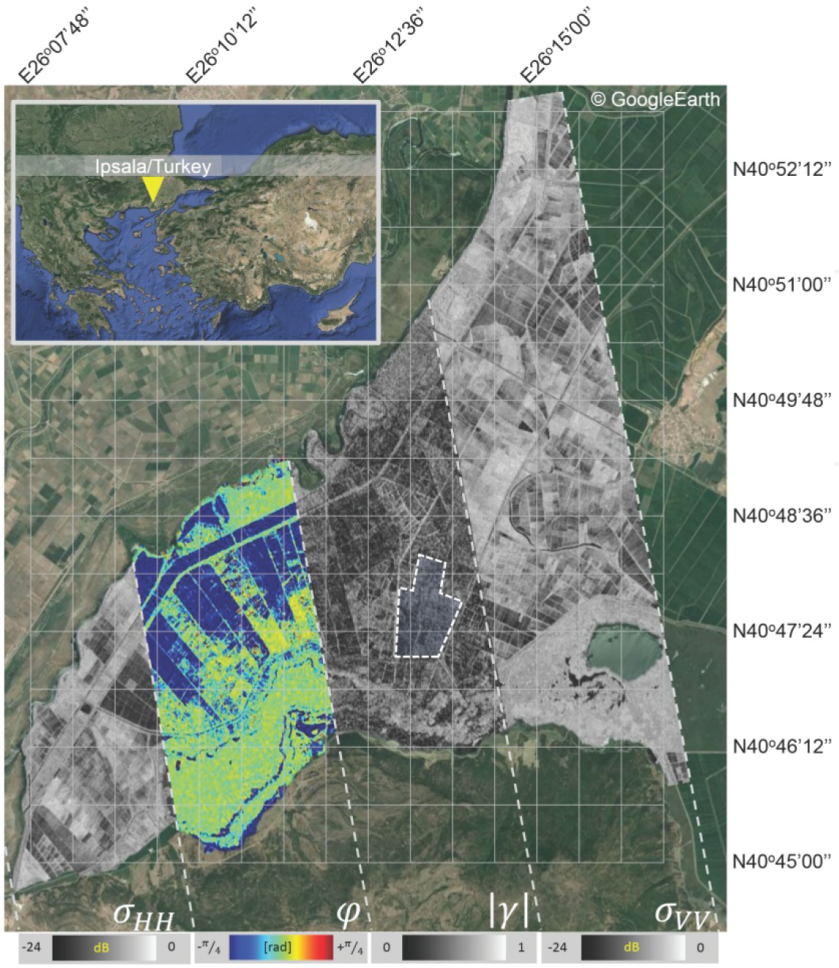

Figure 6. Agricultural study area in Ipsala, Turkey (top-left). Four features are highlighted in the picture [14]. From left to right, over the GoogleEarth image: backscatter in HH polarization, copolar phase difference, copolar coherence, and backscatter in HH polarization. The selected fields for the polarization study performed in Section 4 are highlighted in the coherence portion.

DEMs, for a total of 18 DEMs, with an output raster of 6 m. As shown in **Table 2**, all the rice growing stages in Turkey are covered (May–October), allowing then a temporal study. The height of ambiguity h_a is ranging between about 20 and 30 m. As briefly mentioned in Section 2.1, the relative error can be estimated given the number of looks used in the processing, the coherence, and the ambiguity height. Assuming a coherence value of 0.8 (a reasonable value at the crop locations, as explained in the following) and an independent number of looks of 30, the standard error varies in between 15 cm, as displayed in the last column of **Table 2**. To be noticed, these values refer to a single sample height estimate. The

Major stage	BBCH	Description
Vegetative	00	Germination
	10	Leafing
	20	Tillering
	30	Stem elongation
	40	Booting
Reproductive	50	Heading
	60	Flowering
	70	Fruiting
Maturation	80	Ripening
	90	Senescence

Table 1. BBCH-scale of the rice plant.

Acquisition date (DOY)	Perpendicular baseline [m]	Height of ambiguity [m]	Horizontal resolution [m]	Standard error [cm]
12.05.2012 (133)	253.7	23.1	10.2	36
14.06.2012 (166)	242.3	24.2	10.3	38
06.07.2012 (188)	234.3	25.1	10.2	40
17.07.2012 (199)	227.2	25.8	10.3	41
28.07.2012 (210)	222.7	26.3	10.2	42
19.08.2012 (232)	213.4	27.4	10.3	43
10.09.2012 (254)	204.4	28.7	10.3	46
13.10.2012 (297)	187.1	31.3	10.3	50
26.11.2012 (331)	181.3	32.3	10.3	51

Note: The standard error in the last column is computed for a fixed coherence value of 0.8 and an independent number of looks of 30.

Table 2. Main parameters of the TanDEM-X data set.

independent number of looks of 30 comes from the actual data processing, where a total of 45 looks have been used in the interferogram generation stage (9 in the range and 5 in the azimuth dimensions), and about 30% and 12% of the azimuth and range bandwidth has been filtered out after the spectral shift filter operation [9]. The acquisition mode of the imagery is the standard stripmap one, with a ground range pixel spacing of about 1.5 m and an azimuth one of about 2.5 m. The resulting horizontal resolution, according to Eq. (2), is displayed in the fourth column of **Table 2**. This multilooking operation is a necessary step to reduce the phase noise and the standard height error to a decimetric level for the single pixel

estimate. As aforementioned, due to the relatively smooth topography of the scenes, phase unwrapping is not creating artifacts (even for small height of ambiguities), i.e., no unwrapping errors have been detected. To ensure a straightforward temporal analysis, all the DEMs have been generated using the same output grid and have been equally calibrated using a corrected version of SRTM with ICESat data.

3.3. Field segmentation

In the context of precise farming it is substantial to define field borders that are usually changing every cultivation period. Water management pattern is a further asset useful to supplier. Thus, crop segmentation is mandatory for a field-by-field uncertainty assessment, reasonably assuming a consistent growing within single fields. For this purpose, the interferometric coherence is an important subproduct to exploit, supporting the segmentation algorithm. The adopted strategy is to relate the field segmentation in a water detection problem. Indeed, flooded parcels of land characterize the first phenological phase of the plant. During this state, fields are covered by water and separated by a path network composed by soil or rare grass, as visible also in **Figure 7**, representing the May acquisition. A gravel road network is also present in the test site and separates parcel groups. This natural segmentation is visually detectable by inspecting master channel amplitude in **Figure 7(a)**, as well as the interferometric coherence in **Figure 7(b)**. This visibility relies on the water body dielectric properties. Nonmoving water behaves like a mirror, reflecting the incident signal wave in a specular direction, yielding a very low return to the SAR antenna. This phenomenon brings also a low interferometric coherence. Moreover, it is also known that a water body decorrelates within tens of milliseconds [9] (TanDEM-X small along-track time lags vary between 50 ms (equator) and 0 ms (poles)). The technique proposed by Wendleder et al. [30], operationally employed for the generation of water body mask as an auxiliary product of the official TanDEM-X DEM, is adopted. Specifically, a threshold value of 40 for the amplitude digital number (corresponding to $\sigma^0 = -20$ dB (Eq. (1)) and 0.23 for the coherence (Eq. (5)) were selected. In the study, this strategy is applied for scenes having flooded crops. In **Figure 7**, the May amplitude and coherence data show the flooded parcels for that date with low values. As visible, not all the fields were already flooded (see also **Figure 4**). To better cover the test site, additional information is retrieved by using also two complementary acquisitions taken in May 2013 over the same area.

The sole thresholding operation is not accurate enough to provide a precise segmentation, since fields that are closer than the image resolution (about 10 m, **Table 2**) may result in a single segmented field. Thus, a refinement is necessary. Among various filtering strategies, one of the most straightforward and fast, binary morphology, is chosen [13]. More in detail, erosion with a square (3×3) element is first performed to the binary water mask to remove artifacts, followed by a shape fill to remove holes within the detections. Afterward, the segmentation is performed. A total of more than 2000 fields are detected. The water detection, morphological filtering, and segmentation are performed in the geocoded (geographical coordinates) domain, in order to easily compare them with ground truth data.

(a) amplitude

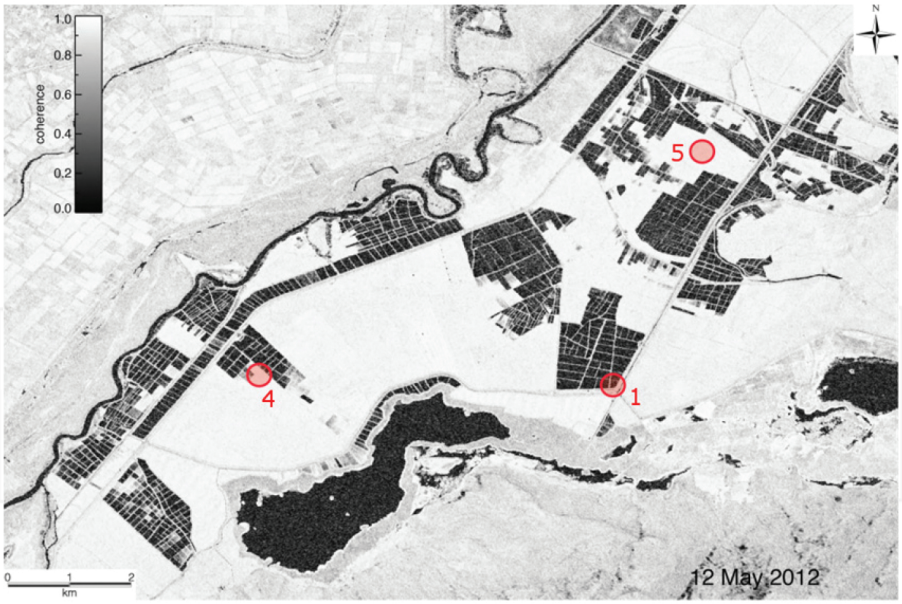

(b) coherence

Figure 7. SAR master channel amplitude (a) and interferometric coherence (b) of the 12.05.2012 TanDEM-X acquisition, used to extract field shapes.

http://dx.doi.org/10.5772/65868

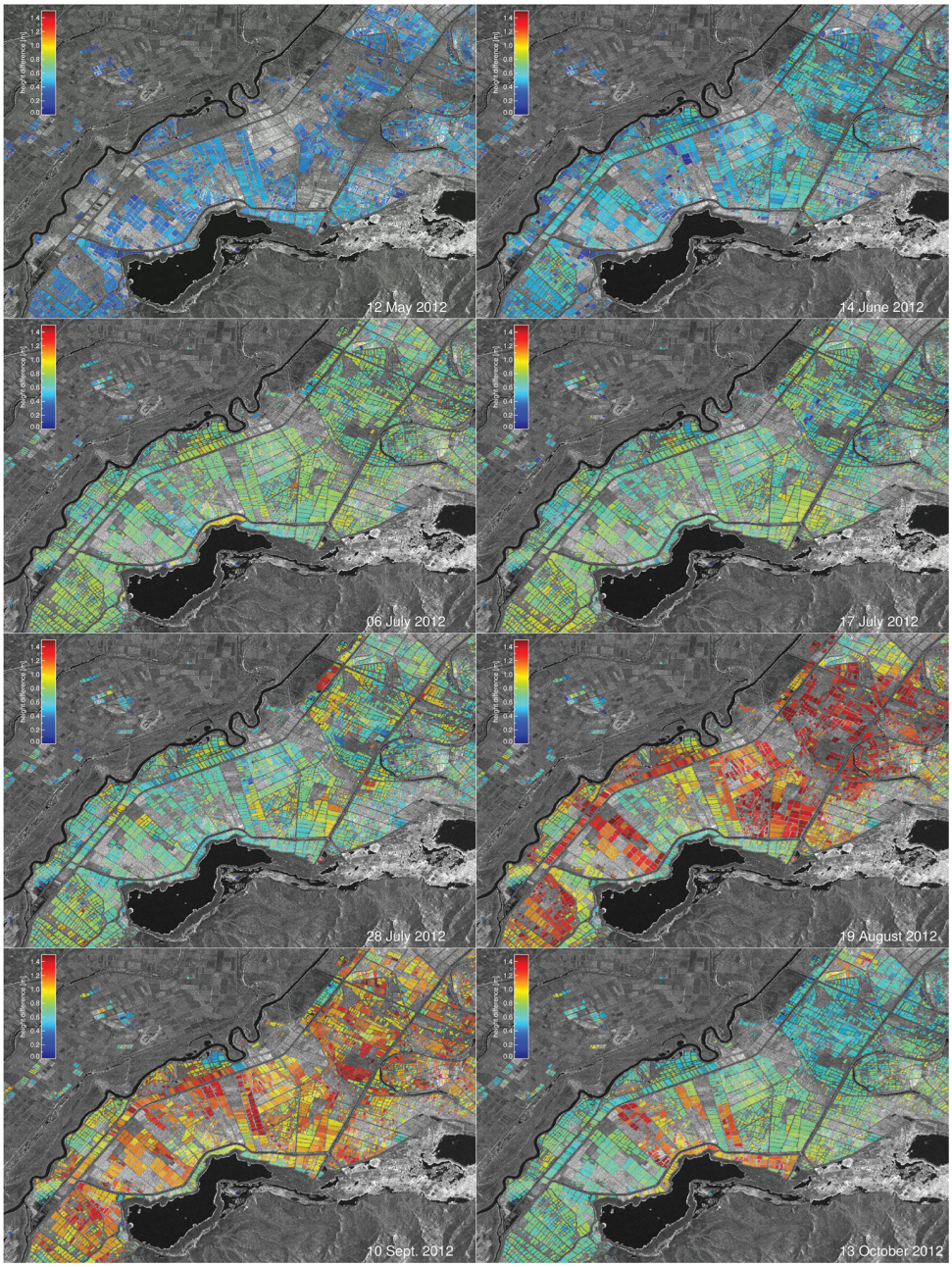

Figure 8. Temporal rice plant heights for the data stack derived with a difference between the DEM generated for the date annotated at the bottom-right and the reference one. The heights are shown in a field-by-field basis, for fields having a mean coherence value higher than 0.8 for both the analyzed and the reference acquisitions.

3.4. Temporal analysis

Since the analysis is on the plant elevation, and the generated DEM is defined over the WGS84 ellipsoid, a reference height corresponding to the plant base must be considered. For that purpose, the last acquisition, in late November, is taken as reference. Indeed, at this acquisition date, the fields have been harvested and the DEM can then be considered as a digital terrain model (DTM), i.e., representing the bare soil elevation. In the following, the November DEM is called for brevity DTM, although this is strictly true only at crop locations. The height difference between the DEMs and the DTM, i.e. the plant heights, is displayed in **Figure 8**, with a single average height value per field. The plant heights are here represented with an overlay between the SAR amplitude and the mean height difference for detected fields, which have an average coherence higher than 0.8 in both the analyzed and the reference acquisitions. A visual analysis of the maps allows the evaluation of the rice plant growth on a field-by-field basis. For instance, the first acquisition shows a limited number of crops since most of them were still flooded. The height of crops is around 20 cm. The numbers of detections increases starting from the second acquisition, i.e., the remaining fields are not flooded anymore, and a visual height growth is noticeable. The growth continues in early July, with a quite homogeneous result with plant heights around 70 cm. The following July maps reveal local changes among fields, e.g., crops located at the northern part grow faster than the ones located at the south. The August map reveals the growing of most of the plants, with doubled heights compared to late June/early July. For some of the fields, the higher maturation level is reached about a month later, as visible in the September map. The mid-October map shows the partial harvesting of some field (to be reminded: a single averaged value is displayed per segmented field), and the full growing for the fields located close to the lake northern coast. In general,

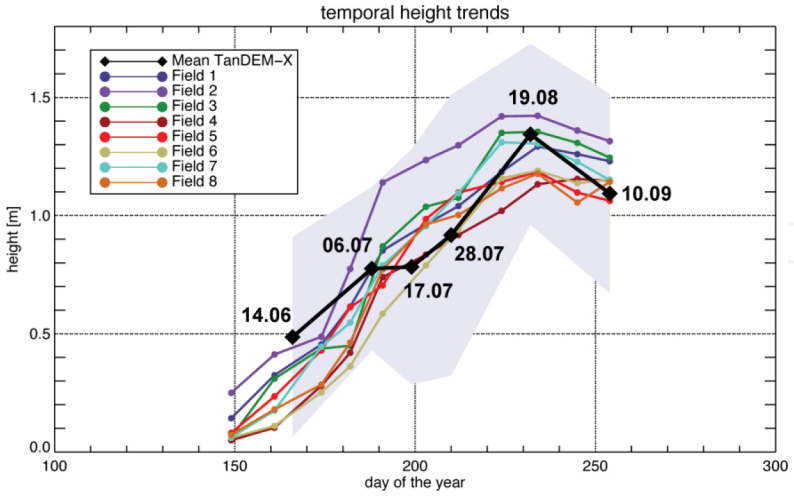

Figure 9. Mean temporal TanDEM-X elevation trend for all the 2012 detected fields over the specific date marked in the plot (black) and corresponding standard deviation (purple). The reference fields are overplotted with colors in the legend.

http://dx.doi.org/10.5772/65868

these maps can be used for the agricultural planning, in terms of production volume and outcomes.

This qualitative inspection already demonstrates the capability to reach the centimetric accuracy necessary to track rice plants. To further highlight it, in **Figure 9** the mean height for the detected fields is shown in black and the standard deviation highlighted in purple. Although crops exhibit variations due to the different seeding dates, the mean height trend exhibits a good accordance with the reference, overplotted in this figure. The height deviation for the late July acquisitions has to be linked to the different growing periods of the detected fields.

The quantitative inspection is performed for three out of eight fields (marked in **Figure 7(b**). The analysis shall link the obtained accuracy derived through a comparison with reference data with the physical characteristics of the plant. The framework is the one delineated in Section 2.2.2. In particular, considering the interferometric analysis, the smaller the extinction, the lower the scattering center (Eq. (4)). Consequently, the retrieved plant elevation will be equal or smaller than the plant top depending on the actual effective dielectric constant of the canopy and the ground, since in the proposed approach the canopy height is retrieved with a difference between a plant growing phase and bare soil.

The differential-InSAR-based and the field-measurement-based canopy height are shown in **Figure 10** in form of scatterplot for three fields. Due to the growing height trend in time, this plot can be easily interpreted. Generally, the elevation trend is well detected by the interferometric measure for the late vegetative phase, reproductive, and maturation stages. Instead, the early vegetative phase represented by the May acquisition yields strongly biased elevation values due to the noisy values originated by the water reflection and is not considered. The plotted heights lie in between mid-June and mid-September (see second to seventh row in **Table 2**).

The June acquisition corresponds to the central vegetative stage (tillering, **Table 1**). At this phase, plants emerge from water (see the second and the third picture in the second row in **Figure 4**). In the SAR resolution cell different phenomena such as direct reflections from water, direct reflections from the surface, and double reflections water-surface (and vice versa) combine together. The interferometric elevation results underestimated due to this combination. The mean difference with reference data results of 7.7 cm for the eight fields taken into consideration in the ground truth campaign. A singular exception is measured for the field 5, marked with blue circles in the scatterplot in **Figure 10**, with an overestimation of about 10 cm. The overestimation has to be attributed to a low mean coherence value (about 0.5), yielding a high phase noise. During this stage, double bounces between growing vegetation and standing water should be the dominant part of the radar return. This implies a scattering phase center located at the water elevation for the cardinal effect on corners—in this case represented by quasi-vertical stems on calm water. However, the small measured height difference suggests the partial presence of the phenomenon due to the use of a short wavelength (3.1 cm) at a relatively high incidence angle (about 37°), yielding a limited penetration of the echo inside the fresh vegetated volume [13]. For the three July measurements the plant elevation exhibits the largest underestimation, with a mean difference of 26.5 cm. Also this discrepancy, at the end of the vegetative stage and beginning of the reproduction (BBCH scale 40–50, **Table 1**), can be explained with the radar wave interaction with the inner part of fresh canopy (see fourth

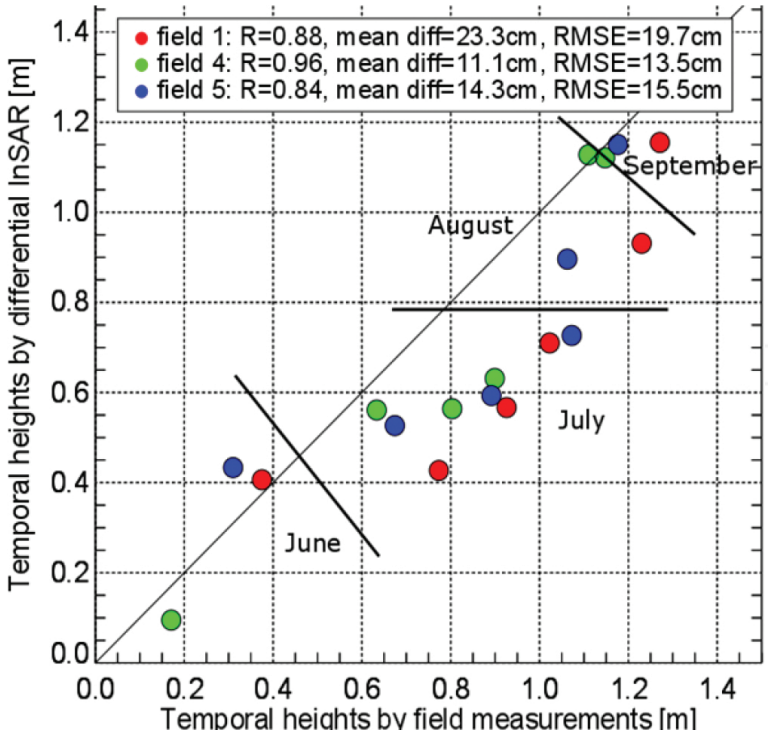

Figure 10. Comparison between interferometric height and ground truth in form of scatterplot for three fields.

picture in the second row in **Figure 4**) and a higher volume decorrelation. The difference in growing can be appreciated for the three fields in the scatterplot, with three different growing rates (higher for field 1, red circles). The August acquisition exhibits instead a generally good matching, with a mean underestimation of 4.8 cm. Being at the beginning of the maturation stage (see fifth picture in the second row in **Figure 4**), plants start to densely produce milky grains at their surface which are the main source of reflection of the signal at X-band. Again, every field should be considered independently due to the structural differences between crops. For instance, field 1 is still in its reproductive stage and shows a scattering phase center about 20 cm below the surface top. The last considered acquisition, in September, falls at the end of the maturation (see seventh picture in the second row in **Figure 4**). The grain is dry and mature, with a maximum height slightly smaller than the previous stage. On this date the interferometric elevations result again underestimated on average, with a mean difference of 16 cm. In principle, at this stage, plant elements are more randomly oriented and drier than in previous ones, hence making more similar the propagation for all polarizations. The aforementioned values represent average values for the eight fields. Just considering the three fields in the plot, the August acquisition reveals actually a higher mismatch than the mean one, while the September acquisition exhibits instead a better match for all the three fields. Once more, this is due to the discrepancies in seeding dates among the fields.

http://dx.doi.org/10.5772/65868

The best fit analysis in the form of $y = ax + b$ in **Figure 10** is used for calculating the offset between the two measurements [13]. As the data time sampling is not overlapping, a linear interpolation for the reference at the InSAR locations is performed. The two sources result highly correlated, with a correlation coefficient R equal to 0.88, 0.96, and 0.84 for the three fields under analysis. The mean differences and root mean square errors are in the decimetric level. In detail, the mean differences between reference and InSAR result 23.3, 11.1, and 14.3 cm and the RMSE (Eq. (5)) 19.7, 13.5, and 15.5 cm for field 1, 4, and 5, respectively. Even though the scattering analysis and the quantitative evaluation performed on this section are useful to understand the overall process, the focus shall be on the centimeter accuracy of the system for this application, and its capability of temporarily tracking the elevation through most of all the growing stages of paddy-rice fields.

Finally, the mean interferometric coherence, proportional to the relative height error (Section 2.2.3) is displayed in **Figure 11**. The mean coherence values for the selected fields are high, with values above 0.8 for all the dates. The only exceptions are for May, when fields are flooded, and for the late July acquisition, when the volume decorrelation reaches its maximum. This contribution linearly increases in July, but is strongly diminished in August, when reflections at the surface top dominates. As a reference, the last column of **Table 2** shows the height error for a fixed coherence value of 0.8.

To characterize the final relative height accuracy, one must consider that the estimated plant height is derived through a difference of two DEMs, implying a standard deviation equal to the sum in quadrature of the standard deviations of the studied DEM and the DTM. Thus, in principle, it is important to ingest an accurate as possible DTM for the algorithm proposed. Considering the chapter case, the DTM, representing bare soil at field locations, is highly accurate, with a mean coherence of about 0.9 (**Figure 11**) and a corresponding relative height

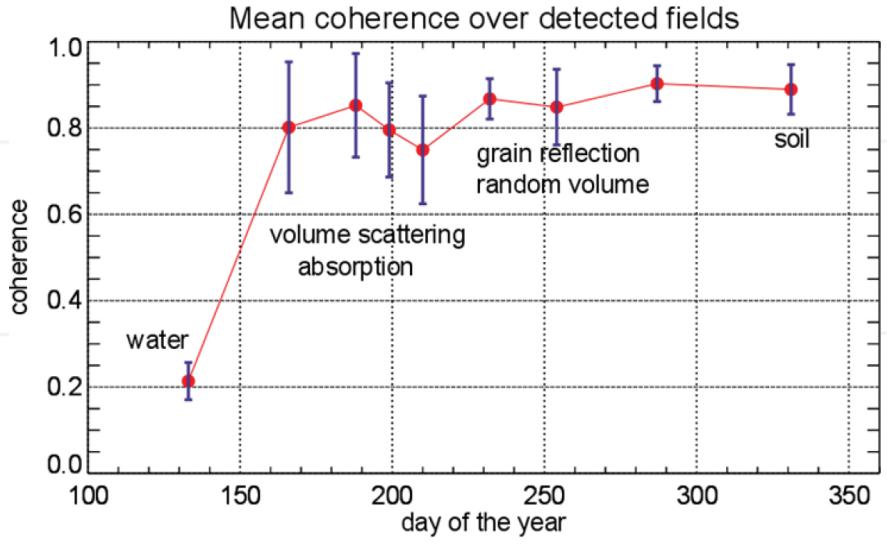

Figure 11. Interferometric mean coherence trend for the detected fields.

error of about 30 cm. Actually, a single height value is derived per field, thus dramatically reducing the overall relative height error of a factor depending on the number of samples composing the crop (fields may span more than 1000 SAR pixels).

4. Impact of wave polarization

The results and discussion provided in the previous section have been derived using the horizontal (HH) polarization and demonstrated the possibility of estimating the height (and derive the phenological stage) of the fields from TanDEM-X data with no additional ground measurements. In this section, the vertical (VV) polarization is studied, with the purpose to study the differences and possibly recommend the *best polarization* for crop monitoring.

In **Figure 12** the interferometric coherence is plotted for the HH and VV channels for the 30 randomly selected fields marked in **Figure 6**. An evident visual divergence appears for the late vegetative-early reproductive stage (around mid-July). Here, the HH elevation accuracy is larger than the VV one, since coherence values are higher (Section 2.2.3). Standard deviation is also smaller for the horizontal polarization. Thus, when considering assessing crop elevation with bistatic data for the central growing stage, it seems advantageous to privilege the HH channel. The two other stages perform similarly: early vegetative has very low coherence and poor elevation estimates for both channels, whereas late reproductive and maturation perform well.

To better characterize the polarization impact in the crop height estimates, the mean elevation difference between differently polarized DEMs for the sample fields is displayed in **Table 3**, together with the elevation standard deviation. For the first date, while fields are flooded, the copolar elevation difference measurement is very large because of the noisy phase information. For the other acquisitions the elevation differences are smaller, below 10 cm.

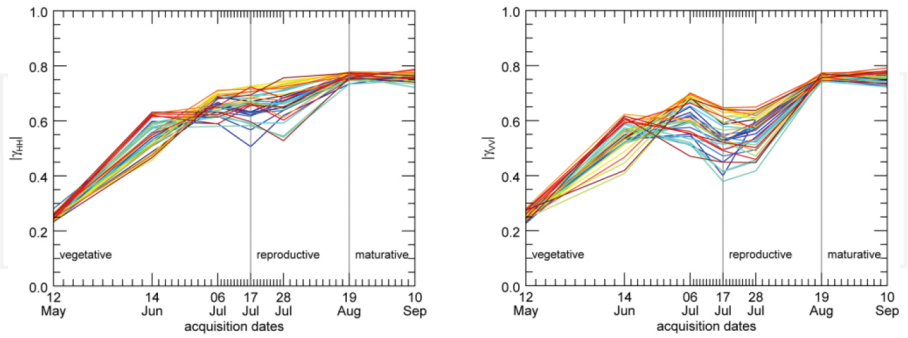

(a) HH coherence (b) VV coherence

Figure 12. Multitemporal coherence measurements from TanDEM-X HH (a) and VV (b) channels along the plan growth cycle for 30 different fields [14].

Acquisition date (DOY)	Sample mean [cm]	Sample STD [cm]
12.05.2012 (133)	+84	204
14.06.2012 (166)	−1	23
06.07.2012 (188)	−3	8
17.07.2012 (199)	−3	11
28.07.2012 (210)	−9	19
19.08.2012 (232)	−8	7
10.09.2012 (254)	−5	10
13.10.2012 (297)	+2	7
26.11.2012 (331)	0	6

Table 3. Copolar height difference statistics between HH and VV channels. The second column displays the mean height difference for 30 randomly selected fields, while the third column displays the standard deviation of the crop elevations for the two polarizations.

The analysis of **Table 3** allows an empirical evaluation of the effect of the extinction coefficient in the vertical channel through almost all the phenological stages. Excluding the first date, the temporal mean difference measurements increase monotonically until late July, i.e., the horizontally polarized signal penetrates more into the canopy compared to the vertically polarized one. The penetration discrepancy is in average of only 1 cm when the plant starts leafing, of 3 cm during tillering, and of 9 cm around the end of the vegetative stage. After, they decrease monotonically until when the plant starts to collapse and to lose its vertical structure. In particular, the measured discrepancy is still close to the maximum while reproduction and slowly decrease while flowering and finally maturing. The sample standard deviations for each acquisition date show the variability of the outcomes for each phenological stage. Values are nearly stable through maturation stage, but in vegetative and reproductive stages they are relatively high considering also the differences in growing rate.

Concluding, horizontal polarization yields digital elevation models with lower crop heights, up to about 10 cm differences. Vertical polarization yet yields higher elevation models, i.e., close to the true top canopy elevation. As aforementioned, horizontal polarization provides, on the average, more accurate elevation results for the central growing stage. So, which is the best polarization for crop elevation monitoring? Generally, if the objective is the determination of the crop elevation, local field coherence should be the final trigger. Nevertheless, for more reliable phenological stage estimation simply based on height, the VV channel can be preferred since it yields higher phase centers, therefore, better modeling the top of the canopy.

5. Conclusions

This chapter underlined the potential of TanDEM-X in paddy-rice elevation mapping. The outcomes can also be an input for the production estimation in terms of volumetric changes.

This is particularly remarkable, considering that the plant tracking requires a centimetric accuracy level and the TanDEM-X specifications are in the order of meters. The uncertainty study demonstrated three major points:

1. For the first time, plant growing has been *directly* measured from a spaceborne SAR system. As outlined in the introduction, previous demonstrations (e.g., ERS in TanDEM configuration) *indirectly* derived the elevation from coherence decomposition. The production of elevation models with InSAR has been reviewed with a special focus on the mapping of agricultural crops. An important point for the study is the presence of a DTM, in order to precisely derive plant heights. In this study, it has been shown how a postharvesting acquisition, and consequently a generated DEM, can serve for the purpose. A straightforward technique to derive field borders, with a simple thresholding operation followed by a refinement with morphological operators, has also been proposed. This refinement can be further improved for future works, for instance with more complex filtering strategies, such as unsupervised active contours techniques.

2. Also the impact of differential extinction on the crop height estimation by differential interferometry has been first experimentally studied with spaceborne SAR data. Although polarization differences are widely used for PolInSAR/PolSAR studies, and precise phenological stage derivation can be extracted by using different polarizations, it has been here demonstrated how the impact in the DEM is rather small, though still present in the DEMs.

3. Keeping the general view, it is important to carry out uncertainty studies in the temporal dimension. In particular, it has been demonstrated how the accuracy level varies depending on the plant phenological stage. Excluding the early stages, when the fields are flooded and the resulting DEM is not accurate, it has been shown how the accuracy level decreases for the late-vegetative stage, when the volume decorrelation is at its maximum, and increases for the following phenological stages, when reflections from the milky grains at the plant top dominates. An interesting and unexpected result comes from the early stages, when the plant can be assumed as a vertical and thin cylinder and the electromagnetic scattering should be dominated by double-bounces, thus with a scattering phase center at the water/soil level. Instead, the derived DEMs have showed a higher phase center, in between the plant top and the soil, suggesting a limited and not dominant double-bounce effect at X-band for rice paddies seeded by broadcasting, i.e., randomly and not in rows.

Acknowledgements

The rice and wetland monitoring in Turkey project was funded by the Scientific and Technological Research Council of Turkey (TUBITAK project no: 113Y446). TanDEM-X SAR data were supplied by the German Aerospace Center under the project no: XTILAND1476.

Author details

Cristian Rossi

Address all correspondence to: cristian.rossi@gmail.com

German Aerospace Center (DLR), Remote Sensing Technology Institute (IMF), Oberpfaffenhofen, Germany

References

[1] FAO. FAO Rice Market Monitor (RMM) [Internet]. [Accessed: http://www.fao.org/economic/est/publications/rice-publications/rice-market-monitor-rmm/en/]

[2] Shao, Y., Fan, X., Liu, H., Xiao, J., Ross, S., Brisco, et al. Rice monitoring and production estimation using multitemporal RADARSAT. Remote Sensing of Environment, 2001; 76 (3), 310–325.

[3] Chakraborty, M., Manjunath, K. R., Panigrahy, S., Kundu, N., & Parihar, J. S. Rice crop parameter retrieval using multi-temporal, multi-incidence angle Radarsat SAR data. ISPRS Journal of Photogrammetry and Remote Sensing, 2005; 59(5), 310–322.

[4] Wang, C., Wu, J., Zhang, Y., Pan, G., Qi, J., & Salas, W. A. Characterizing L-band scattering of paddy-rice in southeast China with radiative transfer model and multitemporal ALOS/PALSAR imagery. IEEE Transactions on Geoscience and Remote Sensing, 2009;47 (4), 988–998.

[5] Bouvet, A., Le Toan, T., & Lam-Dao, N. Monitoring of the rice cropping system in the Mekong Delta using ENVISAT/ASAR dual polarization data. IEEE Transactions on Geoscience and Remote Sensing, 2009; 47(2), 517–526.

[6] Inoue, Y., Sakaiya, E., & Wang, C. Capability of C-band backscattering coefficients from high-resolution satellite SAR sensors to assess biophysical variables in paddy-rice. Remote Sensing of Environment, 2014; 140, 257–266.

[7] Karam, M. A., Fung, A. K., & Antar, Y. M. Electromagnetic wave scattering from some vegetation samples. IEEE Transactions on Geoscience and Remote Sensing, 1988; 26(6), 799–808.

[8] Yuzugullu, O., Erten, E., & Hajnsek, I. Estimation of rice crop height from X-and C-Band PolSAR by metamodel-based optimization. IEEE Journal of Selected Topics in Applied Earth Observations and Remote Sensing, 2016; 1–11.

[9] Bamler, R., & Hartl, P. Synthetic aperture radar interferometry. Inverse Problems, 1998; 14 (4), R1.

[10] Wegmuller, U., & Werner, C. Retrieval of vegetation parameters with SAR interferometry. IEEE Transactions on Geoscience and Remote Sensing, 1997; 35(1), 18–24.

[11] Engdahl, M. E., Borgeaud, M., & Rast, M. The use of ERS-1/2 tandem interferometric coherence in the estimation of agricultural crop heights. IEEE Transactions on Geoscience and Remote Sensing, 2001; 39(8), 1799–1806.

[12] Krieger, G., Moreira, A., Fiedler, H., Hajnsek, I., Werner, M., Younis, M., & Zink, M. TanDEM-X: A satellite formation for high-resolution SAR interferometry. IEEE Transactions on Geoscience and Remote Sensing, 2007; 45(11), 3317–3341.

[13] Rossi, C.,& Erten, E. Paddy-rice monitoring using TanDEM-X. IEEE Transactions on Geoscience and Remote Sensing, 2015; 53(2), 900–910.

[14] Erten, E., Rossi, C., & Yüzügüllü, O. Polarization impact in TanDEM-X data over vertical-oriented vegetation: The paddy-rice case study. IEEE Geoscience and Remote Sensing Letters, 2015; 12(7), 1501–1505.

[15] Cloude, S. R., & Papathanassiou, K. P. Polarimetric SAR interferometry. IEEE Transactions on Geoscience and Remote Sensing, 1998; 36(5), 1551–1565.

[16] Lopez-Sanchez, J. M., & Ballester-Berman, J. D. Potentials of polarimetric SAR interferometry for agriculture monitoring. Radio Science, 2009; 44(2), 1–20.

[17] Lopez-Sanchez, J. M., Hajnsek, I., & Ballester-Berman, J. D. First demonstration of agriculture height retrieval with PolInSAR airborne data. IEEE Geoscience and Remote Sensing Letters, 2012; 9(2), 242–246.

[18] Szeliski, R. Computer vision: algorithms and applications. Springer Science & Business Media. 2010.

[19] Wehr, A., & Lohr, U. Airborne laser scanning—An introduction and overview. ISPRS Journal of Photogrammetry and Remote Sensing, 1999; 54(2), 68–82.

[20] Murakami, T., Yui, M., & Amaha, K. Canopy height measurement by photogrammetric analysis of aerial images: Application to buckwheat (Fagopyrum esculentum Moench) lodging evaluation. Computers and Electronics in Agriculture, 2012; 89, 70–75.

[21] Yu, X., Hyyppä, J., Kukko, A., Maltamo, M., & Kaartinen, H.Change detection techniques for canopy height growth measurements using airborne laser scanner data. Photogrammetric Engineering and Remote Sensing, 2006; 72(12), 1339–1348.

[22] Hanssen, R. F. Radar interferometry: data interpretation and error analysis (Vol. 2). Springer Science & Business Media. 2001.

[23] Fritz, T., Rossi, C., Yague-Martinez, N., Rodriguez-Gonzalez, F., Lachaise, M., & Breit, H. Interferometric processing of TanDEM-X data. In Geoscience and Remote Sensing Symposium (IGARSS), 2011 IEEE International (pp. 2428–2431). IEEE.

[24] Rossi, C., Gonzalez, F. R., Fritz, T., Yague-Martinez, N., & Eineder, M. TanDEM-X calibrated raw DEM generation. ISPRS Journal of Photogrammetry and Remote Sensing, 2012; 73, 12–20.

[25] Breit, H., Fritz, T., Balss, U., Niedermeier, A., Eineder, M., Yague-Martinez, N., & Rossi, C. Processing of bistatic TanDEM-X data. In Geoscience and Remote Sensing Symposium (IGARSS), 2010 IEEE International (pp. 2640–2643). IEEE.

[26] Rabus, B., Eineder, M., Roth, A., & Bamler, R. The shuttle radar topography mission—A new class of digital elevation models acquired by spaceborne radar. ISPRS Journal of Photogrammetry and Remote Sensing, 2003; 57(4), 241–262.

[27] Rossi, C., & Eineder, M. High-resolution InSAR building layovers detection and exploitation. IEEE Transactions on Geoscience and Remote Sensing, 2015;53(12), 6457–6468.

[28] Touzi, R., Lopes, A., Bruniquel, J., & Vachon, P. W. Coherence estimation for SAR imagery. IEEE Transactions on Geoscience and Remote Sensing, 1999; 37(1), 135–149.

[29] Meier, U., Bleiholder, H., Buhr, L., Feller, C., Hack, H., Heß, M.,& Weber, E. The BBCH system to coding the phenological growth stages of plants–history and publications. Journal of für Kulturpflanzen, 2009; 61(2), 41–52.

[30] Wendleder, A., Wessel, B., Roth, A., Breunig, M., Martin, K., & Wagenbrenner, S.TanDEM-X water indication mask: Generation and first evaluation results. IEEE Journal of Selected Topics in Applied Earth Observations and Remote Sensing, 2013; 6(1), 171–179.

[31] Rossi, C., Minet, C., Fritz, T., Eineder, M., & Bamler, R. Temporal monitoring of subglacial volcanoes with TanDEM-X—Application to the 2014–2015 eruption within the Bárðarbunga volcanic system, Iceland. Remote Sensing of Environment, 2016; 181, 186–197.

INTECH